Journal of Low Temperature Physics, Vol. 123, Nos. 3/4, 2001

Optimal Spectrum for the Borocarbides YNi_2B_2C and $LuNi_2B_2C$

S. Manalo[1] and E. Schachinger[2]

[1] *Institut für Theoretische Physik, J. K. Universität Linz, Altenbergerstr. 69, A-4040 Linz, Austria*
[2] *Institut für Theoretische Physik, Technische Universität Graz, Petersgasse 16, A-8010 Graz, Austria*
E-mail: schachinger@itp.tu-graz.ac.at

(Received November 14, 2000; accepted December 27, 2000)

The concept of an optimal electron–phonon interaction spectral density as an Einstein spectrum which allows to describe all physical properties of a superconductor in an optimal way is developed from Carbotte's original definition of an optimum spectrum. It is shown, using the borocarbides YNi_2B_2C and $LuNi_2B_2C$ as examples, that such a concept is meaningful even for anisotropic systems. An Einstein spectrum is sufficient for clean-limit systems, a 2δ-peak spectrum is better suited for anisotropic systems with impurities.

1. INTRODUCTION

Conventional superconductors are well described by Eliashberg theory[1] which treats superconductivity as a boson-exchange phenomenon. The dominant feature of this theory is the electron–phonon interaction spectral function $\alpha^2F(\omega)$ which can be determined from tunneling experiments[2] or theoretically from band structure calculations. Using such an $\alpha^2F(\omega)$ within Eliashberg theory allows to reproduce the superconducting properties of a conventional superconductor within experimental accuracy and this established the phonons as the exchange boson between the two charge carriers building the Cooper pair in conventional superconductors.

Concentrating on isotropic systems Carbotte[3] developed the concept of an optimum spectrum based on earlier work of Leavens[4] and Mitrović and Carbotte.[5] Such a spectrum can be developed from a theorem which states that for a given strength $A = \int_0^\infty d\omega\, \alpha^2F(\omega)$ of the spectral density

0022-2291/01/0500-0149$19.50/0

$\alpha^2F(\omega)$ the best shape that will maximize the critical temperature T_c is a delta function spectrum

$$\alpha^2F(\omega)_{\text{opt}} = A\delta[\omega - \omega^*(\mu^*)], \tag{1}$$

with the delta function placed at the frequency $\omega^*(\mu^*)$ at which the functional derivative $\delta T_c/\delta\alpha^2F(\omega)$ displays its maximum for a fixed value of the Coulomb pseudopotential μ^*. Carbotte[3] extended this concept to encompass other physical properties such as $2\Delta(0)/k_BT_c$, the zero temperature gap $\Delta(0)$ to T_c ratio, and a number of others. This concept establishes that a relation

$$X = Ax(\mu^*) \tag{2}$$

always exists, where X stands for T_c, $2\Delta(0)/k_BT_c$, etc. and $x(\mu^*)$ is a universal number determined from Eliashberg theory for each property X and which varies only slightly with μ^*.

In essence the optimum spectrum gives information about the phonon frequency important to maximize a certain physical property (such as T_c) of a conventional superconductor. Such a concept is very appealing and it suggests an expansion to the concept of an *optimal* spectrum which is again a delta peak spectrum with a delta peak of strength A at some position $\omega^*(\mu^*)$ both chosen to reproduce all known properties of a superconductor optimally. Such a spectrum will then provide information on the phonon mode most important for a specific superconductor if an $\alpha^2F(\omega)$ cannot be derived from experiment. It can also help to develop an $\alpha^2F(\omega)$ in all cases where the phonon density of states $G(\omega)$ is known.

We would like to put this concept to test using the borocarbides $LuNi_2B_2C$ and YNi_2B_2C for which extensive experimental data exist[6] and for which $G(\omega)$ is known from theoretical work.[7,8] From experimental data of the upper critical field H_{c2} which displays a pronounced upward curvature close to T_c in single crystal[9] and polycrystalline[6] samples we also assume these systems to be anisotropic.[10] Shulga *et al.*[11] explained this upward curvature of $H_{c2}(T)$ close to T_c by considering two bands, one of which being more deeply involved in the transport properties of the compound. The authors utilized an *s*-wave electron–phonon Eliashberg formalism and there is growing evidence that the order parameter in YNi_2B_2C is indeed of *s*-wave symmetry.[12] It is interesting to note in passing that concept introduced by Prohammer and Schachinger[10] is effectively a two-band model described by an anisotropic electron–phonon interaction spectral density.[13,14]

Section 2 of this paper reviews the theoretical background, Sec. 3 discusses the results of our analysis, and, finally, in Sec. 4 our conclusions are drawn.

2. THEORY

The theoretical approach towards a theory of anisotropic polycrystalline superconductors within the framework of Eliashberg theory is based on the separable model for the anisotropic electron–phonon interaction introduced by Markovitz and Kadanoff[15] which was extended by Daams and Carbotte[16] to describe an anisotropic electron–phonon interaction spectral function:

$$\alpha^2F(\omega)_{\mathbf{k},\,\mathbf{k}'} = (1 + a_{\mathbf{k}})\,\alpha^2F(\omega)(1 + a_{\mathbf{k}'}), \tag{3}$$

where $\mathbf{k}$ and $\mathbf{k}'$ are the incoming and outgoing quasi-particle momentum vectors in the electron–phonon scattering process and $a_{\mathbf{k}}$ is an anisotropy function with the important feature $\langle a_{\mathbf{k}} \rangle = 0$, where $\langle \cdots \rangle$ denotes the Fermi surface average. As anisotropy effects are generally assumed to be rather small, it is sufficient to keep the mean square anisotropy $\langle a^2 \rangle$ as the important anisotropy parameter. Finally, $\alpha^2F(\omega)$ is the electron–phonon interaction spectral density of the equivalent isotropic system.

Thermodynamic properties of a superconductor are calculated from the free energy difference ΔF between the normal and superconducting state:[17]

$$\Delta F = \pi T N(0) \sum_{n}^{\omega_c} \left\langle (\sqrt{\tilde{\omega}_{\mathbf{k}}^2(\omega_n) + \tilde{\Delta}_{\mathbf{k}}^2(\omega_n)} - |\tilde{\omega}_{\mathbf{k}}(\omega_n)|) \times \left(1 - \frac{|\tilde{\omega}_{\mathbf{k}}^0(\omega_n)|}{\sqrt{\tilde{\omega}_{\mathbf{k}}^2(\omega_n) + \tilde{\Delta}_{\mathbf{k}}^2(\omega_n)}}\right)\right\rangle, \tag{4}$$

with the quasiparticle density of states $N(0)$ at the Fermi level, the renormalized quasiparticle frequencies $\tilde{\omega}_{\mathbf{k}}(\omega_n)$ and the Matsubara gaps $\tilde{\Delta}_{\mathbf{k}}(\omega_n)$ which are the solutions of the nonlinear s-wave Eliashberg equations:

$$\tilde{\omega}_{\mathbf{k}}(\omega_n) = \omega_n + \pi T \sum_{m}^{\omega_c} \left\langle \left(\lambda_{\mathbf{k},\,\mathbf{k}'}(m-n) + \delta_{m,\,n}\,\frac{t^+_{\mathbf{k},\,\mathbf{k}'}}{T}\right) \times \frac{\tilde{\omega}_{\mathbf{k}'}(\omega_m)}{\sqrt{\tilde{\omega}_{\mathbf{k}'}^2(\omega_m) + \tilde{\Delta}_{\mathbf{k}'}^2(\omega_m)}}\right\rangle' \tag{5a}$$

$$\tilde{\Delta}_{\mathbf{k}}(\omega_n) = \pi T \sum_{m}^{\omega_c} \left\langle \left(\lambda_{\mathbf{k},\,\mathbf{k}'}(m-n) - \mu^*_{\mathbf{k},\,\mathbf{k}'} + \delta_{m,\,n}\,\frac{t^+_{\mathbf{k},\,\mathbf{k}'}}{T}\right) \times \frac{\tilde{\Delta}_{\mathbf{k}'}(\omega_m)}{\sqrt{\tilde{\omega}_{\mathbf{k}'}^2(\omega_m) + \tilde{\Delta}_{\mathbf{k}'}^2(\omega_m)}}\right\rangle'. \tag{5b}$$

The $\omega_{\mathbf{k}}^0(\omega_n)$ are the normal state quasiparticle frequencies determined by

$$\tilde{\omega}_{\mathbf{k}}^0(\omega_n) = \omega_n + \pi T \sum_m^{\omega_c} \left\langle \lambda_{\mathbf{k},\mathbf{k}'}(m-n) + \delta_{m,n} \frac{t_{\mathbf{k},\mathbf{k}'}^+}{T} \right\rangle' \operatorname{sgn} \omega_m. \tag{6}$$

In these equations ω_c, the cutoff frequency, is usually an integer multiple of the Debye frequency of the system, $\omega_n = \pi T(2n+1)$, $n = 0, \pm 1, \pm 2, \ldots$, $t_{\mathbf{k},\mathbf{k}'}^+ = 1/(2\pi(\tau_{tr})_{\mathbf{k},\mathbf{k}'})$ is the anisotropic scattering rate due to inelastic impurity scattering with $(\tau_{tr})_{\mathbf{k},\mathbf{k}'}$ as the anisotropic transport relaxation time, $\mu_{\mathbf{k},\mathbf{k}'}^*$ is the anisotropic Coulomb pseudopotential, and

$$\lambda_{\mathbf{k},\mathbf{k}'}(m-n) = 2 \int_0^\infty d\Omega \frac{\Omega \alpha^2 F(\Omega)_{\mathbf{k},\mathbf{k}'}}{\Omega^2 + (\omega_m - \omega_n)^2}. \tag{7}$$

In case of weak anisotropy effects the $\mathbf{k}, \mathbf{k}'$ dependence of the Coulomb pseudopotential and of the impurity scattering is neglected and the anisotropy of the Matsubara gaps is described by the ansatz

$$\tilde{\Delta}_{\mathbf{k}}(\omega_n) = \tilde{\Delta}_0(\omega_n) + a_{\mathbf{k}} \tilde{\Delta}_1(\omega_n), \tag{8}$$

with $\tilde{\Delta}_{0,1}(\omega_n)$ being isotropic functions. In applying Eq. (8) to Eqs. (5) only terms of the order of $\langle a^2 \rangle$ are kept.

The upper critical field $H_{c2}(T)$ of an anisotropic polycrystalline superconductor employs, in addition, a separable ansatz to describe the anisotropy of the Fermi velocity $v_{F,\mathbf{k}}$[10]

$$v_{F,\mathbf{k}} = (1 + b_{\mathbf{k}}) \langle v_F \rangle, \tag{9}$$

with $\langle v_F \rangle$ the isotropic Fermi velocity. $b_{\mathbf{k}}$ is an anisotropy function defined in the same way as $a_{\mathbf{k}}$. Again, only terms of the order $\langle b^2 \rangle$ are kept in case of small anisotropy effects. The upper critical field in its temperature dependence is then described by the following set of equations:[10]

$$\tilde{\Delta}_{\mathbf{k}}(\omega_n) = \pi T \sum_m (1 + a_{\mathbf{k}}) \lambda(m-n) \langle (1 + a_{\mathbf{k}'}) \tilde{\Delta}_{\mathbf{k}'}(\omega_m) \chi_{\mathbf{k}'}(m) \rangle'$$

$$- \pi T \sum_m \left((\mu^* - \delta_{n,m} \frac{t^+}{T}) \langle \tilde{\Delta}_{\mathbf{k}'}(\omega_m) \chi_{\mathbf{k}'}(m) \rangle', \right. \tag{10a}$$

$$\chi_{\mathbf{k}}(n) = \frac{2}{\sqrt{\alpha_{\mathbf{k}}}} \int_0^\infty dx \, \mathrm{e}^{-x^2} \tan^{-1} \left(\frac{\sqrt{\alpha_{\mathbf{k}}}\, x}{|\tilde{\omega}_{\mathbf{k}}(\omega_n)|} \right), \tag{10b}$$

and

$$\alpha_{\mathbf{k}} = \frac{e}{2} H_{c2}(T)(1 + b_{\mathbf{k}})^2 \langle v_F \rangle^2. \tag{11}$$

3. DATA ANALYSIS

3.1. The $\alpha^2F(\omega)$ Spectra

As there are no data available which would allow to determine the electron–phonon interaction spectral density $\alpha^2F(\omega)$ directly by inversion, we have to start our analysis using the phonon density of states $G(\omega)$ which is known from theoretical work.[7, 8] We construct the electron–phonon interaction spectral density using the ansatz

$$\alpha^2F(\omega) = c\omega^s G(\omega), \tag{12}$$

with constants c and s. The coupling strength between electrons and phonons is generally assumed to become weaker with increasing energy ω which leaves s to be negative and it is set to $-1/2$ for simplicity, a value which was also proposed by Junod *et al.*[18] in their analysis of A15-compounds. (Gonnelli *et al.*[12] used instead a two step weighting function which was determined by a fit to the high temperature part of the resistivity of a very pure single crystal YNi_2B_2C sample.) The constant c is then used to rescale the spectrum to obtain the experimentally observed T_c (15.45 K in the case of YNi_2B_2C and 16 K for $LuNi_2B_2C$) using the linearized versions of Eqs. (5) applied to an isotropic system. Figure 1 presents the low energy part of the resulting $\alpha^2F(\omega)$ obtained for a Coulomb pseudopotential $\mu^* = 0.13$. For YNi_2B_2C $\lambda = \lambda(0) = 1.071$ (solid squares) and for $LuNi_2B_2C$ $\lambda = 1.267$ (solid triangles) which identifies both materials as medium coupling strength superconductors.

In the analysis presented here, the actual energy dependence of the $\alpha^2F(\omega)$ spectrum is of no importance as we are going to replace the $\alpha^2F(\omega)$ by an Einstein spectrum with its δ-peak of strength A at some fixed frequency $\omega^*(\mu^*)$ with A and $\omega^*(\mu^*)$ chosen to give the measured T_c, the appropriate value for λ, and the best possible fit to experiment. Nevertheless, these $\alpha^2F(\omega)$ spectra already give a pretty good idea where to place the δ-peak because a quite natural choice is to place the δ-peak at the center of the area under the respective $\alpha^2F(\omega)$ spectrum.

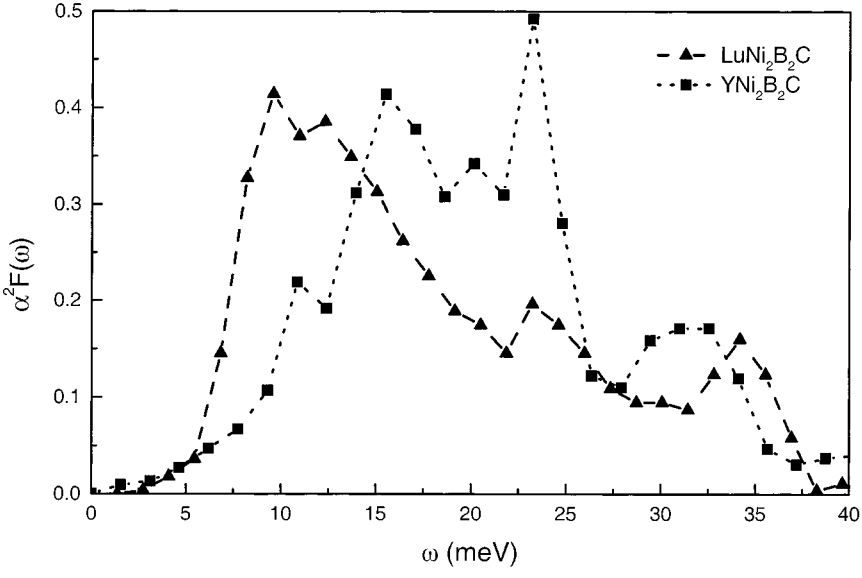

Fig. 1. Spectral densities $\alpha^2F(\omega)$ of $LuNi_2B_2C$ (solid triangles) and YNi_2B_2C (solid squares) in the low-energy range, rescaled to obtain the measured critical temperature T_c for a fixed value of the Coulomb pseudopotential $\mu^* = 0.13$ from the solutions of linearized Eliashberg equations from isotropic systems.

3.2. YNi_2B_2C, Clean-Limit Case

We start the procedure using data for the system YNi_2B_2C and begin with the temperature dependence of the thermodynamic critical field

$$\mu_0 H_c(T) = \sqrt{2\mu_0 \, \Delta F(T)}, \tag{13}$$

with μ_0 the permeability constant of vacuum, and with the deviation function

$$D(t) = \frac{H_c(T)}{H_c(0)} - (1 - t^2), \tag{14}$$

where $t = T/T_c$. The free energy difference $\Delta F(T)$ is determined experimentally by a twofold integration of the specific heat

$$\Delta F(T) = -\int_0^T \int_0^{T'} \mathrm{d}T' \, \mathrm{d}T'' \, \frac{\Delta C(T'')}{T''} \tag{15}$$

measured in magnetic fields between $0 \leqslant \mu_0 H \leqslant 9T$.[6, 19]

The best agreement is found for $\omega^*(\mu^*) = 17$ meV which is close to the center of the area under the $\alpha^2F(\omega)$ spectrum (solid squares, Fig. 1) and a $\lambda = 1.054$. The numerical results obtained from solving Eqs. (5) together with (4) are presented in Figs. 2 and 3 for $H_c(T)$ and $D(t)$ respectively. (We notice the large error bar on the $D(t)$ data points which results from the method used to determine $\Delta F(T)$ from experiment and from the necessary extrapolation of the data to $T \to 0$ to find $H_c(0)$.) Experimental data are shown as open squares, theoretical results are presented for the isotropic case ($\langle a^2 \rangle = 0$, solid line), $\langle a^2 \rangle = 0.01$ (dashed line), $\langle a^2 \rangle = 0.02$ (dotted line), and $\langle a^2 \rangle = 0.03$ (dash-dotted line). It is obvious that results for $0.02 \leqslant \langle a^2 \rangle \leqslant 0.03$ agree best with experiment.

In the next step data for the upper critical field $H_{c2}(T)$ is used to determine the anisotropy parameter $\langle b^2 \rangle$ of the Fermi velocity $\langle v_F \rangle$ within the above range of $\langle a^2 \rangle$ values. Here, the upward curvature of $H_{c2}(T)$ at T_c is used to fit $\langle b^2 \rangle$ while $\langle v_F \rangle$ sets the scale according to Eq. (11). In order to remove ambiguities, an experimental value of the

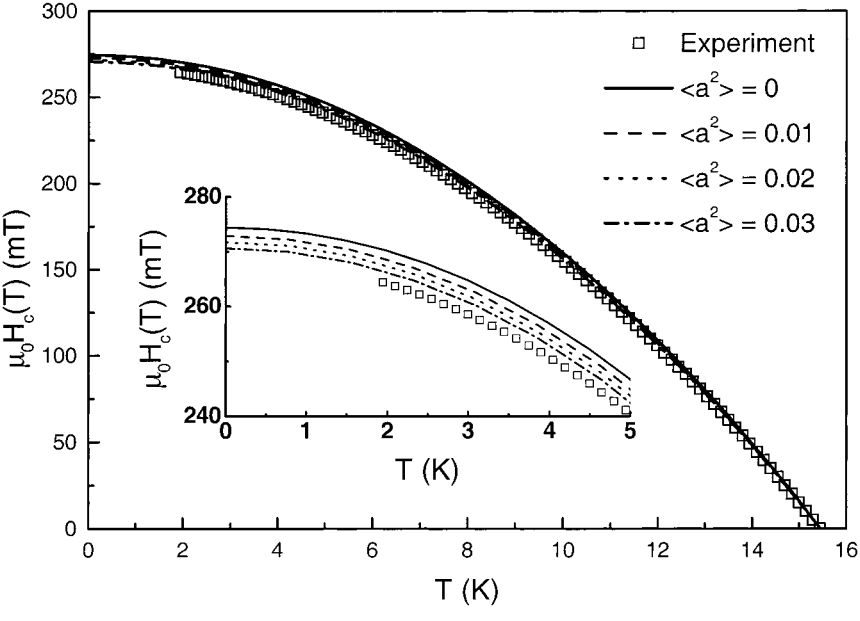

Fig. 2. The temperature dependence of the thermodynamic critical field $H_c(T)$ in YNi_2B_2C, obtained from solutions of the Eliashberg equations (5) for an Einstein spectrum with its δ-peak at $\omega^*(\mu^*) = 17$ MeV and for various anisotropy parameters $\langle a^2 \rangle$, namely $\langle a^2 \rangle = 0$ (isotropic case, solid line), $\langle a^2 \rangle = 0.01$ (dashed line), $\langle a^2 \rangle = 0.02$ (dotted line), and $\langle a^2 \rangle = 0.03$ (dash-dotted line). The open squares represent experimental data.

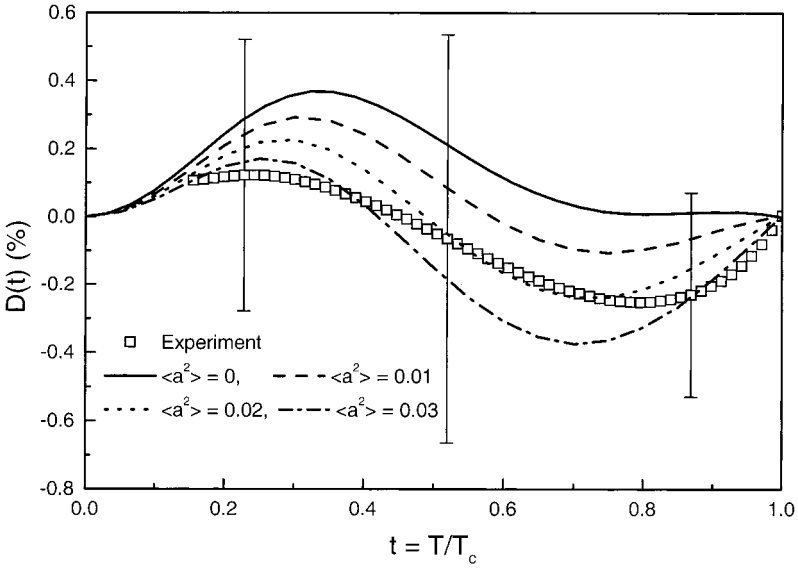

Fig. 3. The thermodynamic critical field deviation function $D(t)$ as a function of the reduced temperature $t = T/T_c$ in YNi_2B_2C, obtained from solutions of the Eliashberg equations (5) for an Einstein spectrum with its δ-peak at $\omega^*(\mu^*) = 17$ MeV and for various anisotropy parameters $\langle a^2 \rangle$, namely $\langle a^2 \rangle = 0$ (isotropic case, solid line), $\langle a^2 \rangle = 0.01$ (dashed line), $\langle a^2 \rangle = 0.02$ (dotted line), and $\langle a^2 \rangle = 0.03$ (dash-dotted line). The open squares represent experimental data.

average Fermi velocity $\langle v_F \rangle$ can be derived from the plasma frequency Ω_p by using

$$h\Omega_p = \sqrt{4\pi e^2 \langle v_F \rangle N(0)/3}. \tag{16}$$

For $LuNi_2B_2C$ $\Omega_p = 4$ meV[20] which results in $\langle v_F \rangle \simeq 0.28 \times 10^6$ m/s. Application of Eqs. (10) with $\langle b^2 \rangle = 0.315$ and $\langle v_F \rangle = 0.275 \times 10^6$ m/s results in the dashed curve in Fig. 7 for $\langle a^2 \rangle = 0.02$ while $\langle b^2 \rangle = 0.305$ and $\langle v_F \rangle = 0.285 \times 10^6$ m/s are found for $\langle a^2 \rangle = 0.03$ (solid line, Fig. 4) to give an optimal fit to experiment (open squares).

The same procedure can be applied to analyze the experimental data of $LuNi_2B_2C$ in a clean limit approach using a single peak Einstein spectrum. The peak is set at the energy $\omega^*(\mu^*) = 15$ meV, again close to the center of area under the $\alpha^2F(\omega)$ spectrum (solid triangles, Fig. 1). The results of such a calculation are presented in Table I and compared to the YNi_2B_2C anisotropy parameters.

This proves that it is indeed possible to describe the features of YNi_2B_2C and $LuNi_2B_2C$ rather well using Eliashberg theory for

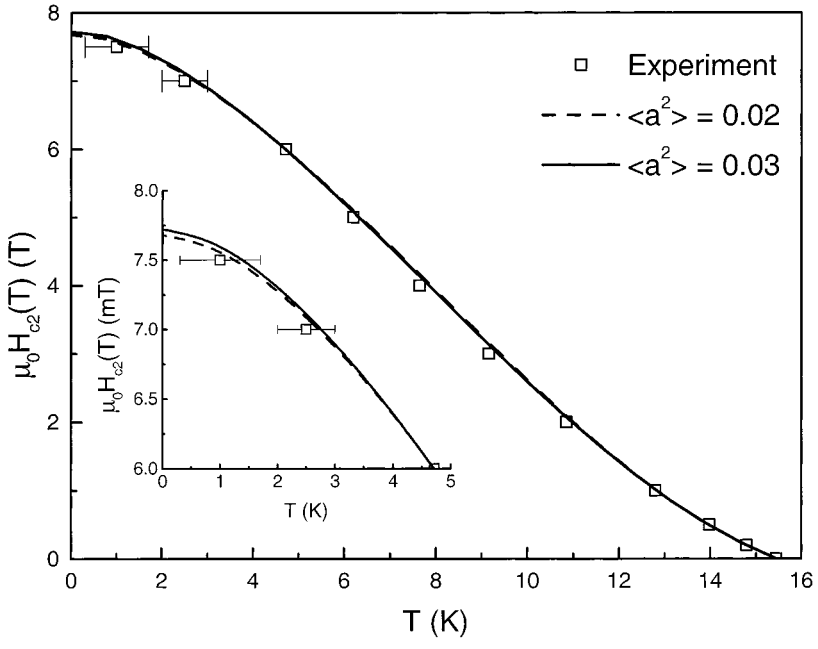

Fig. 4. The temperature dependence of the upper critical field $H_{c2}(T)$ in YNi_2B_2C obtained from solutions of Eqs. (10) for an Einstein spectrum with its δ-peak at $\omega^*(\mu^*) = 17$ MeV and for various anisotropy parameters, namely $\langle a^2 \rangle = 0.02$, $\langle b^2 \rangle = 0.315$, and $\langle v_F \rangle = 0.275 \times 10^6$ m/s (dashed line), and $\langle a^2 \rangle = 0.03$, $\langle b^2 \rangle = 0.305$, and $\langle v_F \rangle = 0.285 \times 10^6$ m/s (solid line). The open squares without visible error bars represent experimental data obtained from specific heat measurements by entropy conservation. The two low temperature data points were determined from resistivity measurements, with error bars indicating the width of the transition.[6]

anisotropic *s*-wave superconductors and a simple Einstein spectrum to describe the energy dependence of the electron–phonon interaction spectral density. Nevertheless, the agreement at low temperatures is still not perfect (see insets of Figs. 2 and 4) which demonstrate that the low temperature data are somewhat overestimated by our analysis.

TABLE I

Anisotropy Parameters for YNi_2B_2C and $LuNi_2B_2C$ from the Clean-Limit Calculations. $\omega^*(\mu^*)$ is in meV, T_c in K, and $\langle v_F \rangle$ in 10^6 m/s

Material	$\omega^*(\mu^*)$	λ	T_c	$\langle a^2 \rangle$	$\langle b^2 \rangle$	$\langle v_F \rangle$
YNi_2B_2C	17.0	1.054	15.45	0.02	0.315	0.275
	17.0	1.054	15.45	0.03	0.305	0.285
$LuNi_2B_2C$	15.0	1.174	16.0	0.02	0.255	0.288
	15.0	1.174	16.0	0.03	0.25	0.298

3.3. Impurity Scattering

In reality, the sample develops some residual resistivity at low temperatures which is an indication of some impurity content. Thus, a clean limit analysis of experimental data as it was presented in the previous subsection can only be a first step which allows to put some margins on the various anisotropy parameters. It would then be standard procedure[21] to load the sample under investigation in a controlled way with some impurities and to measure the change in T_c and in the residual resistivity ρ_n as a function of impurity concentration. This gives another, rather reliable estimate for the anisotropy parameter $\langle a^2 \rangle$[15] and allows to calculate the impurity parameter t^+ which enters Eqs. (5) and (10) from the Drude relation

$$t^+ = \frac{\rho_n h \Omega_p}{8\pi^2}. \tag{17}$$

Such data is not available for YNi_2B_2C and $LuNi_2B_2C$ and we have to develop a different strategy to achieve a more realistic simulation. We make use of the fact that the critical temperature of an anisotropic clean limit system ($t^+ = 0$), T_{c0}, is always greater than the critical temperature of a realistic system with $t^+ > 0$. One can therefore choose a hypothetical value for T_{c0} and calculate how T_c decreases with increasing values of t^+ for a fixed value of $\langle a^2 \rangle$. Results of such a calculation are shown in Fig. 5 (solid line for $T_{c0} = 15.5$ K and $\langle a^2 \rangle = 0.03$, dashed line for $T_{c0} = 15.5$ K and $\langle a^2 \rangle = 0.035$, dotted line for $T_{c0} = 15.55$ K and $\langle a^2 \rangle = 0.035$, and dash-dotted line for $T_{c0} = 15.6$ K and $\langle a^2 \rangle = 0.04$). This defines the value t^+ necessary in the simulation for the realistic system to obtain the experimental value of the critical temperature (labeled T_c, YNi_2B_2C in Fig. 5).

We also have to keep in mind that adding impurities increases $H_{c2}(T)$ even in isotropic systems.[10, 22] Moreover, adding impurities "smears out" the anisotropy[15] which results in increasing values of $H_c(T)$ and an additional increase of $H_{c2}(T)$, and, furthermore, in a less pronounced upward curvature of $H_{c2}(T)$ close to T_c[21] if $\langle a^2 \rangle$ and $\langle b^2 \rangle$ are kept constant in the calculations. Thus, one will have to compensate for adding impurities by an increase of the anisotropy parameters. On the other hand, the anisotropy parameters found for the clean limit system already seem to be rather realistic (they are close to the values given by Manalo *et al.*[6] found by a more elaborate analysis) and we will therefore relay to other means to reestablish agreement with experiment.

Adding a second δ-peak to the $\alpha^2 F(\omega)$ spectrum with its position and strength chosen that, again, the best possible agreement with experiment can be established by changing the anisotropy parameters only minimally

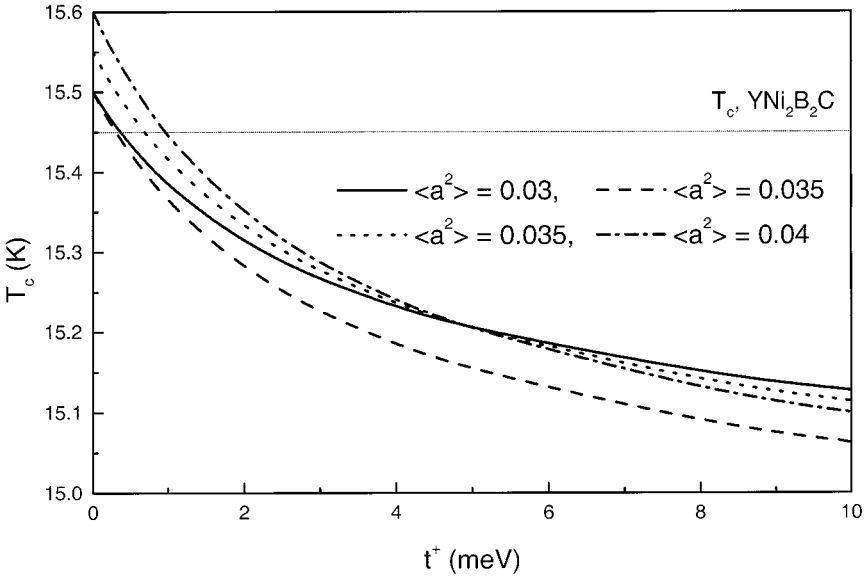

Fig. 5. The critical temperature T_c of an anisotropic superconductor as a function of t^+ which is proportional to the impurity concentration for fixed values of the anisotropy parameter $\langle a^2 \rangle$. The solid line is for $T_{c0} = 15.5$ K and $\langle a^2 \rangle = 0.03$, the dashed one for $T_{c0} = 15.5$ K and $\langle a^2 \rangle = 0.035$, the dotted one for $T_{c0} = 15.55$ K and $\langle a^2 \rangle = 0.035$, and the dash-dotted one for $T_{c0} = 15.6$ K and $\langle a^2 \rangle = 0.04$. The thin straight line labeles T_c and indicates the experimental value of the critical temperature of our YNi_2B_2C sample.

is suggested by functional derivatives $\delta H_{c2}(T)/\delta \alpha^2 F(\omega)$.[23] In particular, functional derivatives reveal that adding spectral weight at high energies to the $\alpha^2 F(\omega)$ spectrum makes it less effective for $H_{c2}(T)$ at low temperatures while adding spectral weight at low energies has just the opposite effect. At high temperatures $H_{c2}(T)$ is far less sensitive to changes in the spectral weight. This is of importance as our calculations overestimate $H_{c2}(T)$ at low temperatures already for the clean limit system in the case of YNi_2B_2C (Fig. 4). We therefore add some spectral weight at higher energies and a natural choice for the energy ω_2 at which this second δ-peak is to be placed is the energy of the maximum in the $\alpha^2 F(\omega)$ spectrum, i.e., $\omega_2 = 21$ meV for YNi_2B_2C (Fig. 1). The strength A_2 of this second peak is chosen to be a tenth of the strength A of the primary δ-peak. This new 2δ-peak spectrum has then to be rescaled to reproduce the experimental value of T_c for the fixed value $\mu^* = 0.13$. This procedure results in a $\lambda = 1.04$ just marginally smaller than the λ of the Einstein spectrum.

Using this new 2δ-spectrum $H_c(T)$ and $H_{c2}(T)$ are recalculated with the parameters shown in Table II. The results for $H_c(T)$ are presented in

TABLE II

Anisotropy Parameters for an Anisotropic System with Impurities used to Simulate the Experimental Data Found for YNi_2B_2C. t^+ is Given in meV and $\langle v_F \rangle$ in 10^6 m/s

Material	T_{c0}	$\langle a^2 \rangle$	t^+	$\langle b^2 \rangle$	$\langle v_F \rangle$
YNi_2B_2C	15.5	0.03	0.366	0.330	0.288
	15.5	0.035	0.306	0.325	0.293
	15.55	0.035	0.684	0.345	0.295
	15.6	0.04	0.961	0.355	0.301
$LuNi_2B_2C$	16.05	0.03	0.533	0.275	0.305
	16.05	0.035	0.455	0.275	0.31
	16.1	0.035	1.025	0.375	0.318
	16.1	0.04	0.859	0.295	0.32

Fig. 6. We see that the low temperature values of $H_c(T)$ are still slightly overestimated by our model calculations, and the results for $H_{c2}(T)$ (Fig. 7) reveal that $H_{c2}(T)$ is now a bit underestimated at very low temperatures but otherwise the agreement is almost perfect for all sets of impurity and anisotropy parameters.

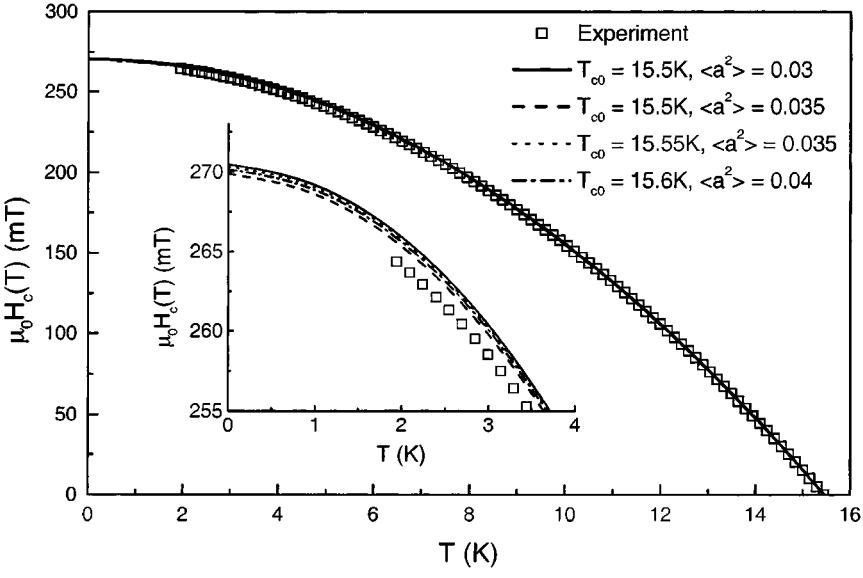

Fig. 6. The temperature dependence of the thermodynamic critical field $H_c(T)$ in YNi_2B_2C, obtained from solutions of the Eliashberg equations (5) for a 2δ-spectrum for the various anisotropy parameters of Table II. The solid line is for $T_{c0} = 15.5$ K and $\langle a^2 \rangle = 0.03$, dashed is for $T_{c0} = 15.5$ K and $\langle a^2 \rangle = 0.035$, dotted is for $T_{c0} = 15.55$ K and $\langle a^2 \rangle = 0.035$, and dash-dotted is for $T_{c0} = 15.6$ K and $\langle a^2 \rangle = 0.04$. The open squares represent experimental data.

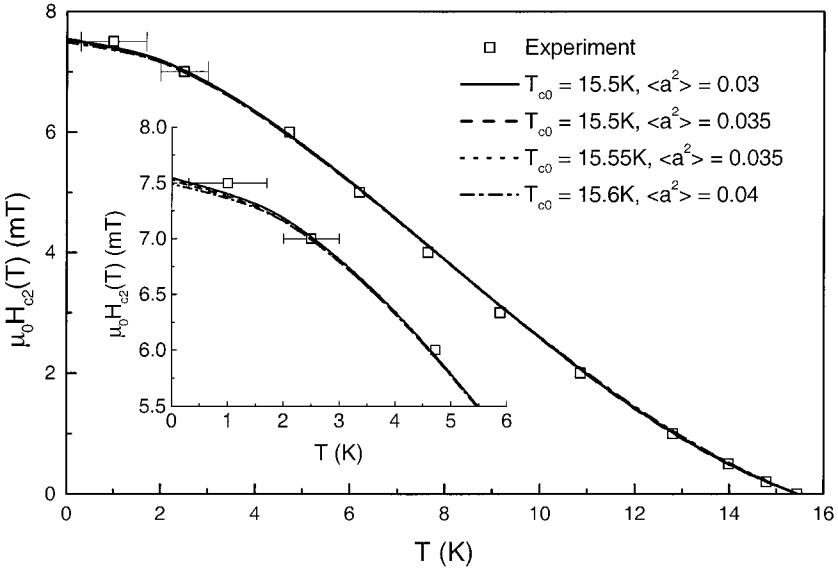

Fig. 7. The temperature dependence of the upper critical field $H_{c2}(T)$ in YNi_2B_2C, obtained from solutions of equations (10) for a 2δ-spectrum for the various anisotropy parameters of Table II. The solid line is for $T_{c0} = 15.5$ K and $\langle a^2 \rangle = 0.03$, dashed is for $T_{c0} = 15.5$ K and $\langle a^2 \rangle = 0.035$, dotted is for $T_{c0} = 15.55$ K and $\langle a^2 \rangle = 0.035$, and dash-dotted is for $T_{c0} = 15.6$ K and $\langle a^2 \rangle = 0.04$. The open squares without visible error bars represent experimental data obtained from specific heat measurements by entropy conservation. The two low temperature data points were determined from resistivity measurements, with error bars indicating the width of the transition.[6]

Again, the same procedure can be applied to the system $LuNi_2B_2C$. We use a 2δ-spectrum with the second peak placed at the maximum in the $\alpha^2F(\omega)$ spectrum (solid triangles, Fig. 1) $\omega_2 = 10$ meV and with its strength given by $A/A_2 \simeq 7.14$ because $H_{c2}(T)$ was originally slightly underestimated. The resulting $\lambda = 1.237$ and the anisotropy parameters for best agreement with experimental data found for this 2δ-spectrum are quoted in Table II.

It is important to emphasize at this point that the agreement between theoretical predictions and experiment is equally good for all sets of parameters quoted in Table II. Thus, only an experiment in which the residual resistivity of the sample is measured can finally help in pinning down the "real" anisotropy parameters. Our analysis only helped to substantially narrow the range of realistic values of the anisotropy parameters.

4. SUMMARY AND CONCLUSION

We investigated two borocarbide systems, namely YNi_2B_2C and $LuNi_2B_2C$, to prove whether the concept of an optimal electron–phonon

interaction spectrum is applicable to anisotropic superconductors in general and to the borocarbides in particular. Such a concept seems to be very helpful if only little is known about the electron–phonon interaction spectral function $\alpha^2F(\omega)$.

This concept is indeed applicable to anisotropic clean limit systems where an Einstein spectrum with its peak placed near the center of the area under a model-$\alpha^2F(\omega)$ spectrum proved sufficient to obtain an excellent agreement between theoretical predictions and experiment over the whole temperature range for thermodynamics and $H_{c2}(T)$. The latter is particularly sensitive to anisotropy effects and details in $\alpha^2F(\omega)$. Nevertheless, even for this property excellent agreement could be achieved. This proves that the model of an anisotropic electron–phonon interaction spectral function $\alpha^2F(\omega)_{\mathbf{k},\mathbf{k}'}$ can be used to explain the upward curvature of $H_{c2}(T)$ close to T_c.

Systems with impurities require compensation of the smearing out of anisotropy by increasing the values of the anisotropy parameters $\langle a^2 \rangle$ and $\langle b^2 \rangle$ if the Einstein spectrum concept is to be extended even to this case. This could result in rather big values for these parameters and in unrealistic values of $\langle v_F \rangle$ necessary to reproduce $H_{c2}(T)$ on an absolute scale. As a way out of this problem we offer to allow the optimal spectrum to be a 2δ-spectrum with the position of the main peak determined from clean limit calculations. Our analysis suggests various critical temperatures T_{c0} for the clean-limit system which is the "origin" of the realistic sample. Measuring the residual resistivity of the sample under investigation will then determine t^+ which in turn gives the appropriate anisotropy parameters (see Table II).

Finally, the applicability of the concept of an optimal $\alpha^2F(\omega)$ spectrum to the systems YNi_2B_2C and $LuNi_2B_2C$ proved that both are classical *s*-wave electron–phonon superconductors adequately described by an Eliashberg theory of anisotropic superconductors.

ACKNOWLEDGMENTS

The authors want to thank Dr. H. Michor and Prof. G. Hilscher for many fruitful discussions regarding the borocarbides. One of us (S.M.) is also very grateful for their support in obtaining the experimental data used in this work as a part of her Diploma thesis.[6]

REFERENCES

1. G. M. Eliashberg, *Sov. Phys. JETP* **11**, 696 (1960).
2. W. L. McMillan and J. M. Rowell, *Phys. Rev. Lett.* **14**, 108 (1965).
3. J. P. Carbotte, *Rev. Mod. Phys.* **62**, 1027 (1990).

4. C. R. Leavens, *Solid State Commun.* **17**, 1499 (1975).
5. B. Mitrović and J. P. Carbotte, *Solid State Commun.* **40**, 249 (1981).
6. S. Manalo, Diploma thesis, Technische Universität Wien, Karlsplatz 13, 1040 Wien, Austria (1999) unpulished; S. Manalo, H. Michor, M. El-Hagary, G. Hilscher, and E. Schachinger, *Phys. Rev. B* (in print) and cond-mat/9911305.
7. F. Gompf, W. Reichardt, H. Schober, B. Renker, and M. Buchgeister, *Phys. Rev. B* **55**, 9058 (1997)
8. W. Weber, Universität Dortmund, Institut für Theoretische Physik II, Otto-Hahn-Str. 4, D-44221 Dortmund (unpublished).
9. Shi Li *et al.*, *Int. J. Mod. Phys.* **13**, 3725 (1999).
10. M. Prohammer and E. Schachinger, *Phys. Rev. B* **36**, 8353 (1987).
11. V. Shulga, S.-L. Drechsler, G. Fuchs, k.-H. Müller, K. Winzer, M. Heinecke, and K. Krug, *Phys. Rev. Lett.* **80**, 1730 (1998).
12. R. S. Gonnelli, A. Morello, G. A. Ummarino, V. A. Stepanov, G. Behr, G. Graw, V. Shulga, and S.-L. Drechsler, cond-mat/0007033 (unbublished).
13. E. Langmann, *Phys. Rev. B* **46**, 9104 (1992).
14. W. Pitscheneder and E. Schachinger, *Phys. Rev. B* **47**, 3300 (1993).
15. D. Markovitz and L. P. Kadanoff, *Phys. Rev.* **131**, 563 (1963).
16. J. M. Daams and J. P. Carbotte, *J. Low Temp. Phys.* **43**, 263 (1981).
17. J. Bardeen and M. Stephen, *Phys. Rev.* **136**, 1485 (1964).
18. A. Junod, T. Jarlborg, and J. Muller, *Phys. Rev. B* **27**, 1568 (1983).
19. H. Michor, T. Holubar, C. Dusek, and G. Hilscher, *Phys. Rev. B* **52**, 16165 (1995).
20. F. Bommeli, L. Degiorgi, P. Wachter, B. K. Cho, P. C. Canfield, R. Chau, and M. B. Maple, *Phys. Rev. Lett.* **78**, 547 (1997).
21. H. W. Weber, E. Seidl, C. Laa, E. Schachinger, M. Prohammer, A. Junod, and D. Eckert, *Phys. Rev. B* **44**, 7585 (1991).
22. N. R. Werthammer, E. Helfand, and P. C. Hohenberg, *Phys. Rev.* **147**, 295 (1966).
23. F. Marsiglio, M. Schossmann, E. Schachinger, and J. P. Carbotte, *Phys. Rev. B* **35**, 3226 (1987).